Journal of Solid State Electrochemistry (2018) 22:3183–3190
https://doi.org/10.1007/s10008-018-4036-6

ORIGINAL PAPER

Solar-responsive sole TiO_2 nanotube arrays with high photocatalytic activity prepared by one-step anodic oxidation

Liang Hao[1,2,3] · Jiancheng Yan[3] · Lijun Cheng[1,2,3] · Qian Zhao[1,2,3] · Sujun Guan[4] · Zheng Zhu[3] · Yun Lu[5]

Received: 24 January 2018 / Revised: 23 June 2018 / Accepted: 25 June 2018 / Published online: 2 July 2018

Abstract

We prepared sole TiO_2 nanotube arrays (NAs) using one-step and two-step anodic oxidation followed by annealing. These TiO_2 NAs were characterized by X-ray diffraction (XRD), Raman spectrum, scanning electron microscopy (SEM), X-ray photoelectron spectroscopy (XPS), UV-Vis absorption spectrum, photoluminescence spectrum (PL), and contact angle measurement. The XRD and Raman spectra results suggest only anatase TiO_2 phase formed after anodic oxidation followed by annealing. The XPS spectra showed that the surface electron density change in the TiO_2 NAs prepared by one-step anodic oxidation compared to those prepared by two-step one. Therefore, the former could absorb visible light more intensely. The PL and photocurrent measurement proved that the recombination rate of electron-hole pairs was suppressed in the sample prepared by two-step anodic oxidation followed by annealing as the degree of crystallinity increased and crystal defects decreased compared with the sample prepared by one-step anodic oxidation followed by annealing. However, the latter possessed better wettability to water and oil and thereby more active sites. The combined action made the sole TiO_2 NAs prepared by one-step anodic oxidation exhibited rather similar high photocatalytic activity in RhB degradation under the irradiation of simulated solar light to those prepared by two-step one. Therefore, solar-responsive sole TiO_2 NAs with high photocatalytic activity were possible to be prepared.

Keywords TiO_2 nanotube coatings · Anodic oxidation · Photocatalytic activity · Solar light

Introduction

Photocatalysis has been investigated extensively for more than 45 years since Fukushima [1] discovered water splitting and following hydrogen generation from the electrolysis system composed of TiO_2 as anode and Pt cathode as under UV irradiation. Some breakthroughs have also been made [2, 3]. Recently, most works are focusing on the photocatalytic mechanism clarification [4, 5] and the photocatalytic activity improvement of photocatalyst nanoparticles under irradiation of visible light [6–8]. However, the recycling difficulty raised their running costs and therefore obstructed the photocatalysis applications in sewage degradation although the nanoparticles always show excellent photocatalytic activity [9]. Therefore, immobilization of photocatalyst nanoarchitecture seems to be particularly urgent. The immobilization in the form of films or coatings should be one of the most facile methods [10]. Furthermore, photocatalyst films and coatings show a great application potential in air purification, sterilization, and sensor [11–13].

Among the methods to prepare TiO_2 coatings, anodic oxidation exhibits advantages such as simple procedure, commercial feasibility, and relatively high efficiency. More importantly, the as-prepared TiO_2 nanotube (NT) coatings possess excellent photocatalytic activity in the degradation of organic dyes after the following crystallization since TiO_2 NT coatings have large specific area [14], great sunlight harvest ability [15], and fast charge-transfer [16]. However, we still cannot

✉ Liang Hao
haoliang@tust.edu.cn

[1] Tianjin Key Lab of Integrated Design and On-line Monitoring for Light Industry & Food Machinery and Equipment, Tianjin, China

[2] International Joint Research Center of Low-Carbon Green Process Equipment, Tianjin, China

[3] College of Mechanical Engineering, Tianjin University of Science & Technology, No. 1038 Dagu Nanlu, Hexi District, Tianjin 300222, China

[4] Department of Physics, Tokyo University of Science, No. 1-3 Kagurazaka, Shinjuku-ku, Tokyo 162-8601, Japan

[5] College of Mechanical Engineering & Graduate School, Chiba University, 1-33, Yayoi-cho, Inage-ku, Chiba 263-8522, Japan

use TiO_2 NT coatings into practical applications due to its relative low visible-light-responsive photocatalytic activity derived from its large band gap and fast hole-electron recombination [4]. Therefore, people have attempted to narrow the band gap by doping them with metallic ions including Zr^{4+} [17], Fe^{3+} [18], Ti^{3+} [19] or with non-metallic ions such as B [20], N [20, 21], and C [21, 22] and among others. In addition, coupling with semiconductors including Cu_2O [23], Ag_2O [24], La_2O_3 [25], or with noble metallic nanoparticles such as Ag [26], Pt [27], and Au [28] is also an effective method. However, the enhancement on photocatalytic activity always accompanied by complicated procedure, and thereby high producing cost. In addition, scientists and engineers have tried their best to prepare perfect morphologies of TiO_2 NTs coatings through two-step anodic oxidation [29–31]. The two-step anodic oxidation also increases the preparation cost. We have to prepare TiO_2 coatings with high photocatalytic activity through facile anodic oxidation at the lowest possible cost before we could use them practically. One-step anodic oxidation becomes an inevitable choice without doubt.

In the present work, we prepared sole TiO_2 NT coatings with facile one-step anodic oxidation and compared the photocatalytic activities of the TiO_2 NT coatings prepared by one-step and two-step anodic oxidation under the irradiation of a weak simulated solar light. The research findings can guide the preparation of solar light-responsive TiO_2 NT coatings with high photocatalytic activity and their practical applications in organic pollutants.

Experimental

Preparation of TiO_2 NAs

TiO_2 NAs are prepared by a facile anodic oxidation method. The preparation process is described as follows. Firstly, Ti foils (30 mm × 20 mm × 0.127 mm, 99.7%, Alfa Aesar) are cleaned in HCl (5 mol/L), ethanol, and deionized water sequentially and separately for 10 min using ultrasonic bath. The cleaned Ti foils are then dried in air at room temperature. Secondly, anodic oxidation is performed in a home-made electrolytic cell with the cleaned Ti foil as the anode and Pt foil (20 mm × 20 mm × 0.025 mm, 99.9%, Alfa Aesar) as the cathode. The electrolyte is composed of ammonium fluoride (1.078 g), deionized water (6 mL), and ethylene glycol (194 mL). The anodic oxidation is conducted at 50 V for 20 min. Finally, the as-prepared samples are immersed in ethanol for 2 h and then dried in air at room temperature. The as-prepared samples need further annealing to drive amorphous TiO_2 NAs crystallization. The samples before and after annealing at 723 K for 2 h with a heating rate of 2 K/min are named as sample A and sample A + H, separately. To investigate the coupling influence of Ag_3PO_4 on photocatalytic activity of TiO_2 NAs, the loading of Ag_3PO_4 nanoparticles on TiO_2 NAs is also conducted by immersing sample A + H into NaH_2PO_4 solution (0.03 mol/L) for 5 min and then transferring to $AgNO_3$ solution (0.05 mol/L) holding for 5 min. The dipping-treated samples are then washed with deionized water. The above dipping treatment is repeated for five times. The as-prepared sample is denoted as A + H + I.

To compare the photocatalytic activity of TiO_2 NAs prepared by one-step and two-step anodic oxidation, we also performed two-step anodic oxidation to make the morphology of TiO_2 NAs perfect. The detailed process is as follows. The Ti foil coated with TiO_2 NAs prepared by one-step anodic oxidation is immersed into deionized water immediately after the first anodic oxidation, and then it is cleaned in ultrasonic bath to peel the formed TiO_2 NAs. One-second-step anodic oxidation was conducted in the same electrolyte at 50 V for 30 min. The as-prepared sample after the above annealing is labeled 2A + H. All the as-received chemical reagents were analytical grade ones.

Characterization

The crystal information of the as-prepared samples A, A + H, A + H + I, and 2A + H is given by X-ray diffraction (XRD, D8 Advance, Bruker, Germany) and Raman spectrometer (DXR Microscope, Thermo Fisher Scientific, USA). The surface morphologies and cross sections of the as-prepared samples are observed using scanning electron microscopy (SEM, Sigma 300, Zeiss, Germany). The surface element analysis is performed with X-ray photoelectron spectroscopy (XPS, Escalab 250Xi, Thermo Fisher Scientific, USA). The UV-Vis absorption spectroscopy is recorded using an UV-Vis spectrophotometer (UV 3600 Plus, Shimadzu, Japan) in the wavelength range of 300~900 nm. The recombination of light-induced electron-hole pairs is examined by photoluminescence spectrometer (PL, iHR320, Horiba, Japan). Photocurrent density was measured with an electrochemical workstation (CHI 650E, Chenhua Co. Ltd., China) using 0.1 mol/L Na_2SO_4 as the electrolyte. The contact angle measurement of the as-prepared samples to water and oil (vacuum pump oil) is performed using contact angle meter (DSA30, Krüss, Germany).

Evaluation of photocatalytic activity

Before photocatalytic activity evaluation of the as-prepared samples, all the samples are cleaned in deionized water and dried in air. The as-prepared samples are then irradiated with UV light for 1 h to degrade residual organic pollutants. A commercially available organic dye rhodamine B (RhB) is chosen as the target pollutant. The photocatalytic RhB degradation is performed under the irradiation of a simulated solar light (CEL-HXF 300, Aulight Co. Ltd., China) with the

optical power density of 45 mW/cm^2, which is smaller than half the AM1.5 of 100 mW/cm^2. RhB molecular adsorption-desorption equilibrium is achieved through the placement in the darkness for 30 min before the evaluation. The concentration of RhB solution is monitored using a UV-Vis spectrophotometer (DR3900, Hach, USA).

Results and discussion

Identification of crystal phases

The XRD patterns of the as-prepared samples are illustrated as shown in Fig. 1. We can observe the diffraction peaks of Ti (marked with symbol T), while the diffraction peaks of anatase or rutile TiO_2 cannot seen in the sample after the anodic oxidation (Fig. 1a). The intensive peaks of anatase TiO_2 appeared in sample A + H (Fig. 1b), which means that amorphous TiO_2 formed in the anodic oxidation and amorphous TiO_2 transferred to anatase TiO_2 in the following annealing. The result is consisted with the reported works [32–34]. Furthermore, the (210) plane diffraction peak of Ag_3PO_4 was also observed in sample A + H + I, which indicates that the dipping method made Ag_3PO_4 particles adhered to TiO_2 NAs. In addition, we can also see that more intensive (101) plane diffraction peak of anatase TiO_2 in sample 2A + H. It suggests that anatase TiO_2 crystals with higher crystallinity degree formed in the sample prepared by two-step anodic oxidation followed by annealing. Figure 2 shows the Raman spectroscopy of the as-prepared samples. Any peak cannot be found in sample A, while intensive peaks at 144, 394, 516, and 635 cm^{-1} are observed in the other samples. According to references [35, 36], the peaks correspond to four Raman active modes of anatase TiO_2 E_g, B_{1g}, A_{1g}, and E_g, respectively. The result confirmed the conclusion obtained from Fig. 1.

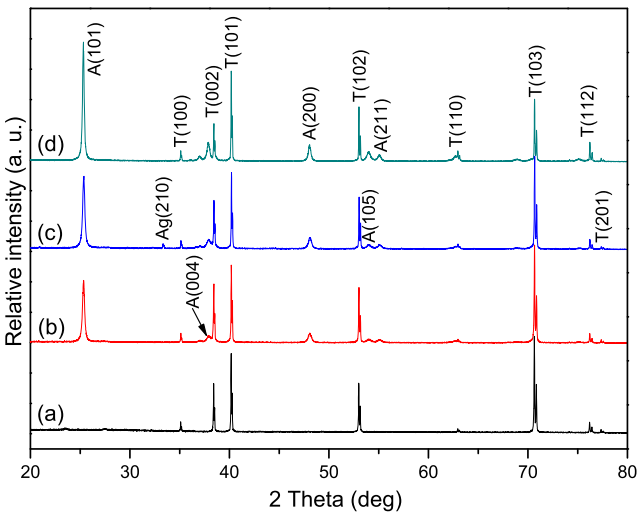

Fig. 1 XRD patterns of the as-prepared samples: **a** A, **b** A + H, **c** A + H + I, and **d** 2A + H

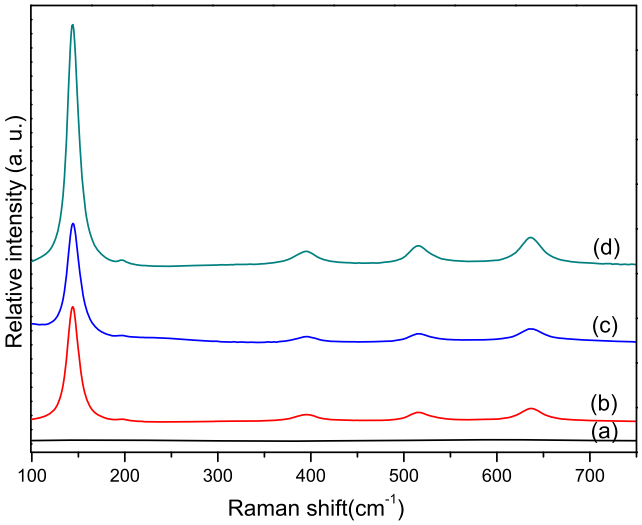

Fig. 2 Raman spectroscopy of the as-prepared samples: **a** A, **b** A + H, **c** A + H + I, and **d** 2A + H

Morphologies and cross sections

Figure 3 shows the morphologies and cross sections of the as-prepared samples. We can see that TiO_2 NAs decorated with some nanoparticles have formed in sample A (Fig. 3a), and the average thickness of the coatings is about 4 μm (Fig. 3c). With energy dispersive spectrometer (EDS) analysis, the decorated nanoparticles is determined to be TiO_2 ones, which peeled off after ultrasonic cleaning. We also noted that the morphology and cross section of the TiO_2 NAs hardly changed after annealing at 723 K except the disappearance of TiO_2 nanoparticles (Fig. 3b, d). With further dipping treatment in $AgNO_3$ and NaH_2PO_4 solution, Ag_3PO_4 nanoparticles formed and adhered to the TiO_2 NAs and they still reserved even experienced ultrasonic cleaning (Fig. 3e, g). It indicates the adhesion of Ag_3PO_4 nanoparticles to the coatings should be firm enough. The SEM images of the morphology and cross section of the sample prepared by two-step anodic oxidation followed by annealing (sample 2A + H) are shown in Fig. 3f, h, respectively. The cracking of the formed TiO_2 NAs is rather evident, and the thickness of the coatings should be a bit greater than sample A + H since the duration of anodic oxidation prolonged.

Photocatalytic activity

Photocatalytic degradation of RhB under the irradiation of weak simulated solar light (45 mW/cm^2) was monitored with the results shown in Fig. 4. With the increase in irradiation time, the concentration of RhB aqueous solution decreased except the one without TiO_2 NAs (blank). It indicates that RhB does not degrade under the irradiation of simulated solar light. For all the RhB aqueous solutions with TiO_2 NAs, their concentrations decreased to an almost same value after

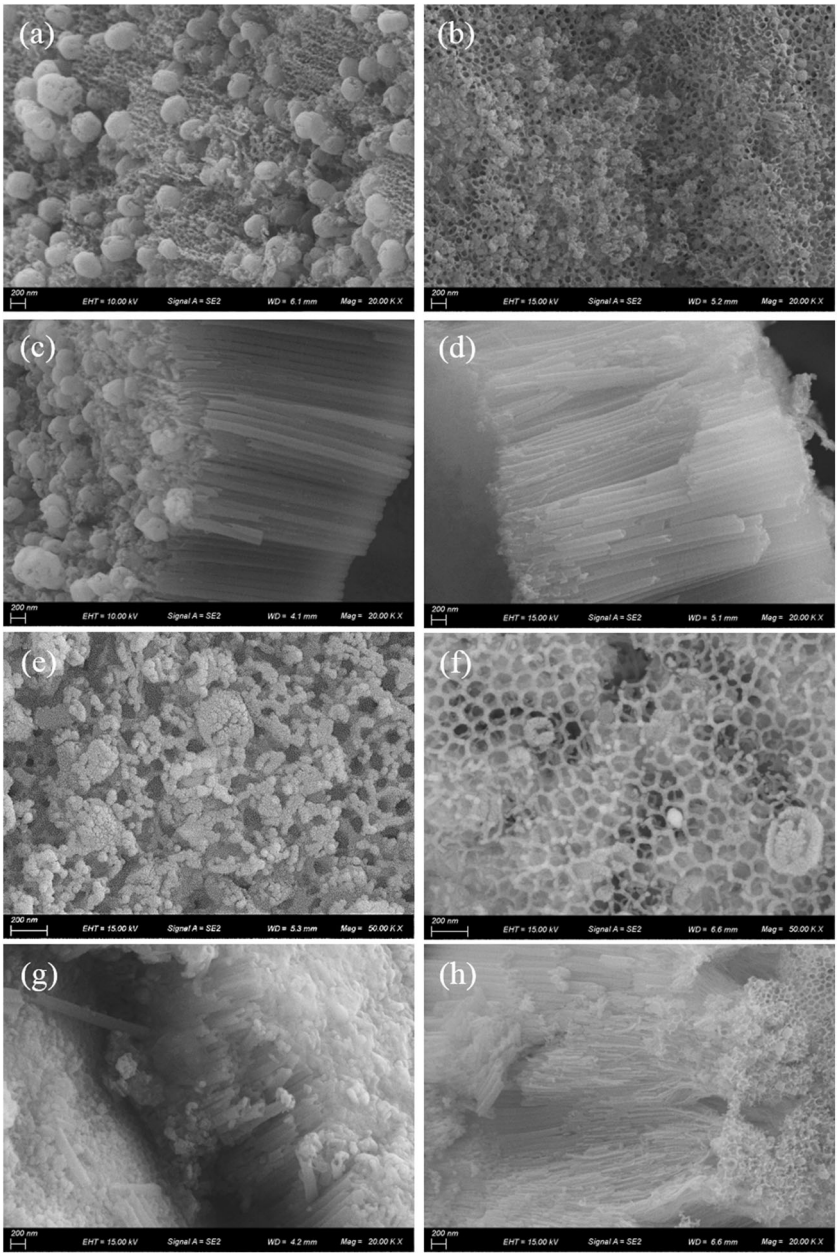

Fig. 3 SEM images of the morphologies and cross sections of the as-prepared samples: **a**, **c** A; **b**, **d** A + H; **e**, **g** A + H + I; **f**, **h** 2A + H

irradiation of 60 min. It suggests sample A + H, A + H + I and 2A + H exhibited similar photocatalytic performance in the photocatalytic degradation of RhB. However, the photocatalytic activity of sample A + H + I began to drop as the simulated solar irradiation continued although the other two samples A + H and 2A + H still showed high photocatalytic activity during the whole irradiation. The concentration of RhB aqueous solution decreased to 2.2 mg/L, which was about 44% of the initial concentration. What is more, the samples A + H and 2A + H possessed rather similar photocatalytic activity during the whole process. In other words, the TiO_2 NAs prepared by one-step anodic oxidation and two-step anodic oxidation showed the similar photocatalytic activity. Therefore, one-step anodic oxidation method is capable of preparing solar-responsive TiO_2 NAs with high photocatalytic activity.

Surface analysis

The XPS spectra of the as-prepared samples are shown in Fig. 5. Figure 5a shows the XPS spectrum of Ti 2p, in which the BE values of Ti 2p3/2 and Ti 2p1/2 of the samples prepared by one-step anodic oxidation located at 459.3 and 465.0 eV, respectively. They show a positive shift of 0.7 eV compared to those of the sample prepared by two-step anodic oxidation. It is reported that the BE values of Ti 2p3/2 and Ti 2p1/2 in TiO_2 NAs usually appears at 458.5 ± 0.4 and 464.2 ± 0.4 eV [37–39]. The XPS information is in good agreement

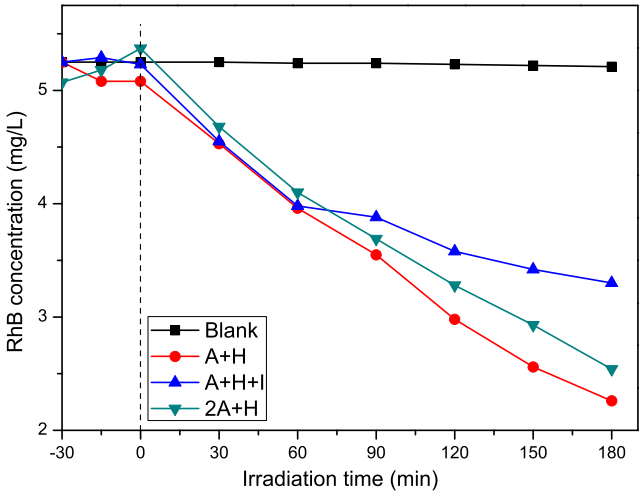

Fig. 4 Degradation of RhB in aqueous solution under the action of the as-prepared samples and simulated solar light irradiation

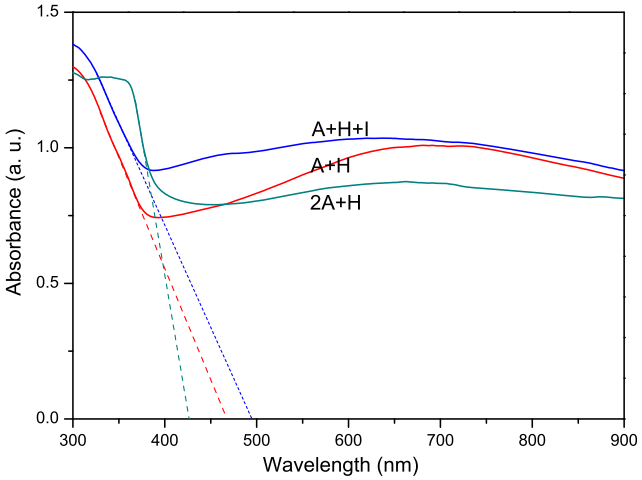

Fig. 6 UV-Vis absorption spectra of the as-prepared samples

with that prepared by two-step anodic oxidation. The shift of the BE values for the samples prepared by one-step anodic oxidation indicates the surface electron density reduce of TiO_2. Figure 5b shows the O 1 s spectra, in which the peak at 529.9 eV of the sample prepared by two-step anodic oxidation correspond to Ti-O. The result fits perfectly the reported values [40, 41]. Three clear peaks at 530.5, 530.6, and 530.7 eV in the samples prepared by one-step anodic oxidation are also confirmed as those of Ti-O bond in TiO_2 [42]. Furthermore, some weak peaks around 532.0 eV are also detected in the samples prepared by one-step anodic oxidation. These peaks correspond to hydroxyl groups or H_2O, which are rather important for enhancing the photocatalytic activity of TiO_2 [43, 44].

Figure 6 shows the optical absorption spectra of the as-prepared samples prepared by one-step and two-step anodic oxidation followed by annealing. We can clearly see that all the samples absorb all colors of light within the wavelength of 300~900 nm. The absorption thresholds of samples A + H, A + H + I, and 2A + H are determined to be about 460, 495, and 430 nm, respectively. From the above values, we calculated the band gaps of these samples to be 2.7, 2.5, and 2.88 eV, respectively. Therefore, the sample prepared by one-step anodic oxidation (A + H) can absorb more visible light than that prepared by two-step anodic oxidation (2A + H). The combination of TiO_2 NAs with Ag_3PO_4 nanoparticles makes the band gap reduce to 2.5 eV and thereby they can absorb visible light more intensively.

Photoluminescence (PL) analysis shown in Fig. 7 are also performed as it could provide powerful information of photogenerated charge carrier behavior of semiconductors [45]. As shown in Fig. 7, all the samples exhibited single obvious PL single peak at a wavelength of 582 nm, which suggests that the annealing, two-step anodic oxidation and the combination with Ag_3PO_4 nanoparticles were not enough to generate a new PL signal. Generally, it is believed that

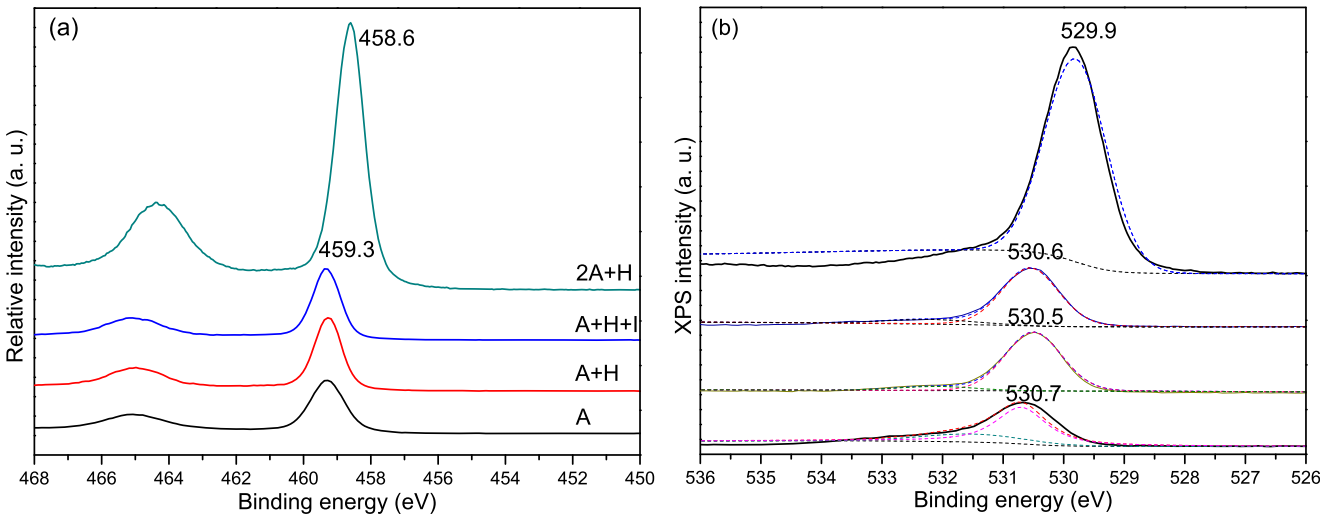

Fig. 5 XPS spectra of the as-prepared samples: **a** Ti 2p and **b** O 1 s

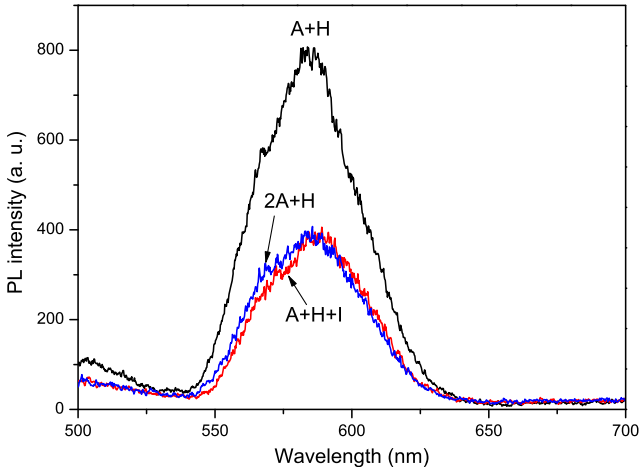

Fig. 7 PL spectra of the as-prepared samples

lower PL intensity means an enhanced separation and transfer of photogenerated electrons trapped in semiconductor [45–48]. Therefore, we consider that the recombination rate of photogenerated hole-electron pairs in samples 2A + H and A + H + I is lower than that in sample A + H.

Figure 8 shows the transient photocurrent response of the as-prepared samples under the irradiation of simulated solar light. We noted that the photocurrent density of sample A + H was rather faint even can be negligible. The faint photocurrent density should ascribe to the high recombination rate of photogenerated hole-electron pairs. After the coupling with Ag_3PO_4 nanoparticles, the recombination of hole-electron pairs were evidently suppressed which resulted in a great photocurrent density value as observed in Fig. 8. In addition, the photocurrent density of sample 2A + H was also much greater than that of sample A + H.

The absorption of dye molecules to the photocatalyst surface is the first step of photocatalytic degradation. Therefore, the wettability of TiO_2 NAs to water and oil is rather important to their photocatalytic degradation performance of RhB in

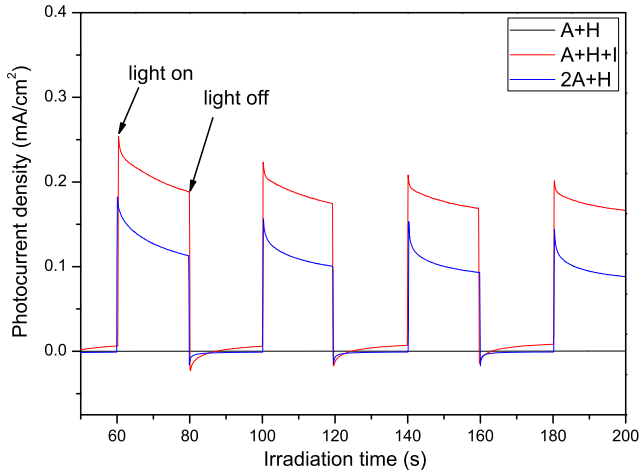

Fig. 8 Transient photocurrent response of the as-prepared samples under simulated solar light irradiation

aqueous solution [49]. Table 1 shows the contact angles of the as-prepared samples to water and oil. It can be clearly seen that sample A + H shows smaller contact angles to water and oil than samples 2A + H and A + H + I. It indicates that sample A + H can absorb more water and RhB molecules than samples A + H + I and 2A + H.

Generally, the TiO_2 NAs prepared by two-step anodic oxidation followed by annealing possess more perfect morphologies, higher specific area, and greater crystallinity, thereby better photocatalytic performance [50–52]. Therefore, people have tried their best to prepare TiO_2 NT coatings with perfect morphologies through two-step anodic oxidation although it takes more cost and complicated procedure. In this work, the TiO_2 NAs prepared by one-step anodic oxidation followed by annealing (sample A + H) showed an extremely similar photocatalytic activity in the degradation of RhB under the irradiation of weak simulated solar light comparing to those prepared by two-step anodic oxidation (sample 2A + H). It means we can prepare TiO_2 NAs with higher photocatalytic performance at lower cost, which can greatly promote their practical applications in industrial sewage treatment, air purification, and among others. As for the similar photocatalytic performance of the samples prepared by one-step and two-step anodic oxidation, we present some analysis and discussion as follows.

The photogenerated holes and electrons produce some chemical species including H_2O, OH^- and O_2 to produce •OH, $O_2^{\bullet-}$ and H_2O_2 [53]. However, the contribution of $O_2^{\bullet-}$ in oxidation reactions such as RhB photocatalytic degradation is quite smaller than that of •OH and holes as the amounts of the former are rather small [53, 54]. Therefore, we believe that the amounts of the escaped holes and resulting •OH determine the photocatalytic activity of TiO_2 NT coatings in oxidizing RhB molecules. In other words, all the factors promoting to produce holes and •OH radicals could enhance the photocatalytic activity of TiO_2 NT coatings in degrading RhB. From the results presented by the PL spectra (Fig. 7), the recombination rate of hole-electron pairs in sample A + H was greater than those in samples A + H + I and 2A + H. Therefore, we can safely conclude that the amounts of active oxidizing species to mineralize RhB molecules on the surface of sample A + H is smaller than those of samples A + H + I and 2A + H. The photocurrent response in Fig. 8 also proved our deduction.

Table 1 Contact angles of the as-prepared samples to water and oil

Media sample	Water	Oil
A + H	6.4°	26.3°
A + H + I	18.7°	32.3°
2A + H	13.4°	44.4°

On the other hand, sample A + H could absorb more visible light compared to sample 2A + H in Fig. 6. The enhanced visible light absorption should relate to the surface state change of TiO_2 NAs. From the results in XPS, the positive shift of Ti 2p and O 1 s corresponds to the surface electron density change. It results in more surface defects, which enhanced the visible light absorption. The further enhancement in visible light absorption of sample A + H + I should attribute to the coupling with Ag_3PO_4 nanoparticle [55]. Furthermore, the wettabilities of sample A + H to water and oil are better than those of sample 2A + H (Fig. 8), which means that the surface of sample A + H could absorb more RhB molecules and thereby more active sites.

The above positive factors, such as intensive visible light absorption and better wettabilities to water and oil, and negative factors, including greater recombination rate of hole-electron pairs, and high degree of crystallinity, made sample A + H possess rather similar photocatalytic degradation performance of RhB compared with sample 2A + H.

Conclusions

Sole TiO_2 nanotube arrays (NAs) are prepared by one-step and two-step anodic oxidation followed by annealing. The comprehensive analysis revealed that anatase TiO_2 NAs were formed by anodic oxidation followed by annealing no matter one-step or two-step anodic oxidation. Two-step anodic oxidation increased the degree of crystallinity of TiO_2 and therefore decreased the recombination rate of photogenerated electron-hole pairs compared to one-step anodic oxidation. On the other hand, TiO_2 NAs prepared by one-step anodic oxidation possessed more surface defects and thereby absorbed visible light more intensely compared to the TiO_2 NAs prepared by two-step anodic oxidation. More importantly, the TiO_2 NAs prepared by one-step anodic oxidation exhibited better wettability to water and oil than those prepared by two-step anodic oxidation. The combined action of surface defects, degree of crystallinity, visible light absorption, and wettability to water and oil made the sole TiO_2 NAs prepared by one-step anodic oxidation followed by annealing had rather similar excellent photocatalytic activity in RhB degradation under the irradiation of simulated solar light compared to those prepared by two-step anodic oxidation. Therefore, one-step anodic oxidation is a facile and economic method to prepare solar-responsive TiO_2 NAs with high performance.

Funding information This work is supported by the National Nature Science Foundation of China (No. 51404170), the Scientific Research Foundation of Tianjin University of Science & Technology (No. 10220), and the Innovation Team Program of Tianjin University of Science & Technology (No. 10117).

References

1. Fujishima A, Honda K (1972) Electrochemical photolysis of water at a semiconductor electrode. Nature 238(5358):37–38
2. Asahi R, Morikawa T, Ohwaki T, Aoki K, Taga Y (2001) Visible-light photocatalysis in nitrogen-doped titanium oxides. Science 293(5528):269–271
3. Chen X, Liu L, Yu PY, Mao SS (2011) Increasing solar absorption for photocatalysis with black hydrogenated titanium dioxide nanocrystals. Science 331(6018):746–750
4. Hoffmann MR, Martin ST, Choi W, Bahnemann DW (1995) Environmental applications of semiconductor photocatalysis. Chem Rev 95(1):69–96
5. Linsebigler AL, Lu G, Yates JT (1995) Photocatalysis on TiO_2 surfaces: principles, mechanism, and selected results. Chem Rev 95(3):735–758
6. Lin Z, Li J, Zheng Z, Yan J, Liu P, Wang C, Yang G (2015) Electronic reconstruction of α-Ag_2WO_4 nanorods for visible-light photocatalysis. ACS Nano 9(7):7256–7265
7. Lee K, Kim D, Roy P, Paramasivam I, Birajdar BI, Spiecker E, Schmuki P (2010) Anodic formation of thick anatase TiO_2 mesosponge layers for high-efficiency photocatalysis. J Am Chem Soc 132(5):1478–1479
8. Hu S, Shaner MR, Beardslee JA, Lichterman M, Brunschwig BS, Lewis NS (2014) Amorphous TiO_2 coatings stabilize Si, GaAs, and GaP photoanodes for efficient water oxidation. Science 344(6187):1005–1009
9. Kuo D, Hsu W, Yang Y (2016) From the fluorescent lamp-induced bactericidal performance of sputtered Ag/TiO_2 films to re-explore the photocatalytic mechanism. Appl Catal B Environ 184:191–200
10. Jiang W, Qiu Z, Yao W, Zhu Y, Cui W (2017) TiO_2/$Al(H_2PO_4)_3$ composite film as separation-free and washing-resistance photocatalyst. Appl Catal B Environ 204:3–48
11. Demirci S, Dikici T, Yurddaskal M, Gultekin S, Toparli M, Celik E (2016) Synthesis and characterization of Ag doped TiO_2 heterojunction films and their photocatalytic performances. Appl Surf Sci 390:591–601
12. Luo L, Miao L, Tanemura S, Tanemura M (2008) Photocatalytic sterilization of TiO_2 films coated on Al fiber. Mater Sci Eng B 148(1-3):183–186
13. Rothschild A, Edelman F, Komen Y, Cosandey F (2000) Sensing behavior of TiO_2 thin films exposed to air at low temperatures. Sensors Actuators B Chem 67(3):282–289
14. Ye Y, Feng Y, Bruning H, Yntema D, Rijnaarts HHM (2018) Photocatalytic degradation of metoprolol by TiO_2 nanotube arrays and UV-LED: effect of catalyst properties, operational parameters, commonly present water constituents, and photo-induced reactive species. Appl Catal B Environ 220:171–180
15. Yang Z, Ma Z, Pan D, Chen D, Xu F, Chen S (2014) Enhancing the performance of front-illuminated dye-sensitized solar cells with highly [001] oriented, single-crystal-like TiO_2 nanotube arrays. Ceram Int 40(1):173–180
16. Wang Z, Liu B, Xie Z, Li Y, Shen Z (2016) Preparation and photocatalytic properties of RuO_2/TiO_2 composite nanotube arrays. Ceram Int 42(12):13664–13669
17. Liu H, Liu G, Zhou Q (2009) Preparation and characterization of Zr doped TiO_2 nanotube arrays on the titanium sheet and their photocatalytic activity. J Solid State Chem 182(12):3238–3242
18. Wang Q, Jin R, Zhang M, Gao S (2017) Solvothermal preparation of Fe-doped TiO_2 nanotube arrays for enhancement in visible light induced photoelectrochemical performance. J Alloys Compd 690:139–144
19. Zhu W, Wang C, Chen J, Li Y, Wang J (2014) Enhanced field emission from Ti^{3+} self-doped TiO_2 nanotube arrays synthesized by a facile cathodic reduction process. Appl Surf Sci 301:525–529

20. Georgieva J, Valova E, Armyanov S, Tatchev D, Sotiropoulos S, Avramova I, Dimitrova N, Hubin A, Steenhaut O (2017) A simple preparation method and characterization of B and N co-doped TiO_2 nanotube arrays with enhanced photoelectrochemical performance. Appl Surf Sci 413:284–291
21. Mollavali M, Falamaki C, Rohani S (2015) Preparation of multi-doped TiO_2 nanotube arrays with nitrogen, carbon and nickel with enhanced visible light photoelectrochemical activity via single-step anodization. Int J Hydrog Energy 40(36):12239–12252
22. Liu S, Yang L, Xu S, Luo S, Cai Q (2009) Photocatalytic activities of C-N-doped TiO_2 nanotube array/carbon nanorod composite. Electrochem Commun 11(9):1748–1751
23. Sun Q, Peng Y, Chen H, Chang K, Qiu Y, Lai S (2016) Photoelectrochemical oxidation of ibuprofen via Cu_2O-doped TiO_2 nanotube arrays. J Hazard Mater 319:121–129
24. Deng X, Ma Q, Cui Y, Zhang H, Cheng X, Li X, Cheng M, Li B (2017) Microwave-assisted synthesis of Ag_2O/reduced TiO_2 nanotube arrays photoelectrode with enhanced visible photocatalytic activity for degradation of organic pollutants. Sep Purif Technol 182:230–237
25. Li H, Feng B (2016) Visible-light-driven composite La_2O_3/TiO_2 nanotube arrays: synthesis and improved photocatalytic activity. Mater Sci Semicond Process 43:55–59
26. Kong J, Song C, Zhang W, Xiong Y, Wan M, Wang Y (2017) Enhanced visible-light-active photocatalytic performanced on Ag nanoparticles sensitized TiO_2 nanotube arrays. Superlattice Microst 109:579–587
27. Wang Y, Zhu Y, Zhao X, Yang X, Li X, Chen Z, Yang L, Zhu L, Gao T, Sha Z (2015) Improving photocatalytic Rhodamine B degrading activity with Pt quantum dots on TiO_2 nanotube arrays. Surf Coat Technol 281:89–97
28. Wu L, Li F, Xu Y, Zhang JW, Zhang D, Li G, Li H (2015) Plasmon-induced photoelectrocatalytic activity of Au nanoparticles enhanced TiO_2 nanotube arrays electrodes for environmental remediation. Appl Catal B Environ 164:217–224
29. Cho I, Choi J, Zhang K, Kim S, Jeong M, Cai L, Park T, Park J, Zheng X (2015) Highly efficient solar water splitting from transferred TiO_2 nanotube arrays. Nano Lett 15(9):5709–5715
30. Ye M, Gong J, Lai Y, Lin C, Lin Z (2012) High-efficiency photoelectrocatalytic hydrogen generation enabled by palladium quantum dots-sensitized TiO_2 nanotube arrays. J Am Chem Soc 134(38):15720–25723
31. Koo M, Cho K, Yoon J, Choi W (2017) Photoelectrochemical degradation of organic compounds coupled with molecular hydrogen generation using electrochromic TiO_2 nanotube arrays. Environ Sci Technol 51(11):6590–6598
32. Wang C, Zhu W, Chen J, Hou X, Zhang X, Li Y, Wang J, Zhou F (2014) Low-temperature ammonia annealed TiO_2 nanotube arrays: synergy of morphology improvement and nitrogen doping for enhanced field emission. Thin Solid Films 556:440–446
33. Liao J, Lin S, Zhang L, Pan N, Cao X, Li J (2012) Photocatalytic degradation of methyl orange using a TiO_2/Ti mesh electrode with 3D nanotube arrays. ACS Appl Mater Interfaces 4(1):171–177
34. Kurian S, Seo H, Jeon H (2013) Significant enhancement in visible light absorption of TiO_2 nanotube arrays by surface band gap tuning. J Phys Chem C 117(33):16811–16819
35. Rao BM, Roy SC (2014) Anatase TiO_2 nanotube arrays with high temperature stability. RSC Adv 4(72):38133–38139
36. Krengvirat W, Sreekantan S, Noor AM, Negishi N, Kawamura G, Muto H, Matsuda A (2013) Low-temperature crystallization of TiO_2 nanotube arrays via hot water treatment and their photocatalytic properties under visible-light irradiation. Mater Chem Phys 137(3):991–998
37. Liang H, Li X (2009) Effect of structure of anodic TiO_2 nanotube arrays on photocatalytic activity for the degradation of 2, 3-dichlorophenol in aqueous solution. J Hazard Mater 162(2-3): 1415–1422
38. Li G, Liu Z, Lu J, Wang L, Zhang Z (2009) Effect of calcination temperature on the morphology and surface properties of TiO_2 nanotube arrays. Appl Surf Sci 255(16):7323–7328
39. Guo R, Wang C, Chen J, Wang J, Wang L, Liu W (2010) Field emission from TiO_2/Ti nanotube arrays with different morphologies. Physica B 405(22):4682–4686
40. Si Y, Liu H, Li N, Zhong J, Li J, Ma D (2018) SDBS-assisted hydrothermal treatment of TiO_2 with improved photocatalytic activity. Mater Lett 212:147–150
41. Jiao Z, Shang M, Liu J, Lu G, Wang X, Bi Y (2017) The charge transfer mechanism of Bi modified TiO_2 nanotube arrays: TiO_2 serving as a charge-transfer-bridge. Nano Energy 31:96–104
42. Mazieski P, Nadolna J, Lisowski W, Winiarski MJ, Gazda M, Nischk M, Klimczuk T, Zaleska-Medynska A (2017) Effect of irradiation intensity and initial pollutant concentration on gas phase photocatalytic activity of TiO_2 nanotube arrays. Catal Today 284: 19–26
43. Li M, Guo R, Hu C, Sun P, Pan W, Liu S, Sun X, Liu S, Liu J (2018) The enhanced resistance to K deactivation of Ce/TiO_2 catalyst for NH_3-SCR reaction by the modification with P. Appl Surf Sci 436: 814–822
44. Yu SQ, Ling YH, Wang RG, Zhang J, Qin F, Zhang ZJ (2018) Constructing superhydrophobic WO_3/TiO_2 nanoflake surface beyond amorphous alloy against electrochemical corrosion on iron steel. Appl Surf Sci 436:527–535
45. Wu Q, Ouyang J, Xie K, Sun L, Wang M, Lin C (2012) Ultrasound-assisted synthesis and visible-light-driven photocatalytic activity of Fe-incorporated TiO_2 nanotube array photocatalysts. J Hazard Mater 199-200:410–417
46. Jing L, Qu Y, Wang B, Li S, Jiang B, Yang L, Fu W, Fu H, Sun J (2006) Review of photoluminescence performance of nano-sized semiconductor materials and its relationships with photocatalytic activity. Sol Energy Mater Sol Cells 90:1773–1787
47. Liao W, Wang B, Liu Z (2017) Photoelectrochemical hydrogen production at peak efficiency over 10% via PbSe QDs/TiO_2 nanotube array photoanodes. Int J Hydrog Energy 42(16):10962–10970
48. Wang Y, Li Z, Tian Y, Zhao W, Liu X, Yang J (2014) Facile method for fabricating silver-doped TiO_2 nanotube arrays with enhanced photoelectrochemical property. Mater Lett 122:248–251
49. Li Y, Sasaki T, Shimizu Y, Koshizaki N (2008) Hexagonal-close-packed, hierarchical amorphous TiO_2 nanocolumn arrays: transferability, enhanced photocatalytic activity, and superamphiphilicity without UV irradiation. J Am Chem Soc 130(44):14755–14762
50. Smith YR, Sarma B, Mohanty SK, Misra M (2012) Light-assisted anodized TiO_2 nanotube arrays. ACS Appl Mater Interfaces 4(4): 5883–5890
51. Yu D, Song Y, Zhu X, Yang C, Yang B, Xiao H (2013) Fabrication of bundle-free TiO_2 nanotube arrays with wide open top via a modified two-step anodization process. Mater Lett 109:211–213
52. Peighambardoust N, Nasirpouri F (2013) Manipulating morphology, pore geometry and ordering degree of TiO_2 nanotube arrays by anodic oxidation. Surf Coat Technol 235:727–734
53. Ochiai T, Fujishima A (2012) Photoelectrochemical properties of TiO_2 photocatalyst and its applications for environmental purification. J Photochem Photobiol C 13(4):247–262
54. Hwang S, Petucci C, Raftery D (1998) In situ solid-state NMR studies of trichloroethylene photocatalysis: formation and characterization of surface-bound intermediates. J Am Chem Soc 120(18): 4388–4397
55. Wang Q, Zheng Q, Jin R, Gao S, Yuan Q, Rong W, Wang R (2017) Photoelectrocatalytic removal of organic dyes and Cr (VI) ions using Ag_3PO_4 nanoparticles sensitized TiO_2 nanotube arrays. Mater Chem Phys 199:209–215